Brazilian Journal of Microbiology
https://doi.org/10.1007/s42770-024-01563-z

MEDICINE AND PUBLIC HEALTH - RESEARCH PAPER

# Comparative analysis of biofilm structures in *Salmonella* Typhimurium DMC4 strain and its *dam* and *seq*A gene mutants using Fourier transform infrared spectroscopy (FT-IR) and Raman spectroscopy methods

**Caner Özdemir[1] · İbrahim Erdoğan[2] · Kağan Özdemir[3] · Nefise Akçelik[4] · Mustafa Akçelik[1]**

Received: 3 June 2024 / Accepted: 1 November 2024
© The Author(s) under exclusive licence to Sociedade Brasileira de Microbiologia 2024

## Abstract

It is well-established that the *dam* and *seqA* genes act in the biofilm production in *Salmonella*. However, the molecular basis underlying this activity remains unexplored. This study aims to address this gap in the literature. In this study, comparative Fourier Transform Infrared (FT-IR) Spectroscopy and Raman spectral analyses were conducted to investigate the molecular basis of decreases in swimming, swarming motility, and biofilm characteristics observed in the *dam* and *seqA* gene mutants of *S.* Typhimurium DMC4 wild-type strain. The comparative analysis revealed a pronounced reduction in proteins, lipids, carbohydrates, and nucleic acids within the biofilm structures of mutant strains. These findings confirm that these macromolecules are crucial for the integrity and functionality of biofilm structures. FT-IR analysis showed that while amide-I bands decreased in the biofilm structures of mutant strains, amide-II bands increased compared to the wild-type strain. Similarly, Raman analyses indicated an increase in amide-IV bonds and a decrease in amide-V bonds. The parallelism between FT-IR and Raman spectral analysis results, particularly regarding amide I, amide V, amide II, and amide IV bands, is noteworthy. Additionally, these findings may lead to the development of markers for rapidly diagnosing transitions from planktonic to biofilm form in *Salmonella*. The substantial decrease in β-glucans and lipids, including cellulose, within the biofilm matrix of mutant strains highlights the critical role these polymers play in swimming and swarming motility. Given the clinical and industrial importance of *Salmonella* biofilms, it is crucial to develop strategies to prevent biofilm formation and identify target molecules that can inhibit biofilm formation. The results of our study suggest that β-glucans and amides are essential targets in the effort to combat *Salmonella* biofilms.

**Keywords** *Salmonella* · *Dam* · *seqA* · Biofilm · FT-IR · Raman spectroscopy

## Introduction

*Salmonella* is a leading cause of gastrointestinal foodborne illness worldwide with a global prevalence affecting the gastrointestinal tract. The consumption of raw or undercooked products of animal origin is the main source of *Salmonella* infections. The presence of biofilms occurring in food systems functions as a reservoir by providing a constant presence of *Salmonella* on surfaces that are highly resistant to environmental stress conditions. Consequently, the persistence of these biofilms in food industries may increase the risk of food contamination and human infections [1, 2].

A biofilm is defined as a community of microorganisms tightly attached to a biotic or abiotic surface. These communities are embedded within an extracellular polymeric

Responsible Editor: Juliana Pfrimer Falcão.

✉ Mustafa Akçelik
akcelik@science.ankara.edu.tr

[1] Department of Biology, Ankara University, Ankara, Turkey

[2] Department of Agricultural Biotechnology, Ahi Evran University, Kırşehir, Turkey

[3] Department of Statistics, Ankara University, Ankara, Turkey

[4] Biotechnology Institute, Ankara University, Ankara, Turkey

Published online: 08 November 2024

matrix (EPS), a complex mixture of proteins, carbohydrates, lipids, and nucleic acids. This matrix not only provides structural support but also creates a microenvironment that can significantly alter the characteristics of the microorganisms, including gene expression, protein synthesis, growth rate, and metabolic activities [3]. An important feature that distinguishes this structure from other bacterial communities is the global genetic regulation that occurs in the transition from the planktonic to biofilm form. This transition triggers a shift in the bacteria's behavior and functions, leading to spatial and functional differentiation within the biofilm structure [4]. The EPS matrix plays a crucial role in this process, as it facilitates the organization of bacteria into distinct layers or clusters, each with specialized roles and activities. This structure, which is an integral element of the structural properties and functionality of biofilms, enables the morphotyping of *Salmonella* biofilms. According to this morphotyping performed on nutrient media containing Congo Red, based on whether there are curli fimbriae and cellulose in *Salmonella* biofilm structures, biofilm morphotypes containing both curli fimbriae and cellulose in the EPS structure are rdar (red, dry, rough). The biofilm morphotypes containing only curli fimbriae in the EPS structure are bdar (brown, dry, rough). Biofilm morphotypes containing only cellulose in the EPS structure are defined as pdar (pink, dry, rough) [5]. Accurately determining biofilm morphotypes is of great importance for the resistance of the biofilms produced to adverse environmental conditions and the selection of agents to combat such biofilms [6]. Among these morphotypes, the rdar type is known to be the most resistant to biofilm-fighting agents and other stress conditions. This resistance is partly due to the rigidity added by curli proteins and the additional elasticity provided by cellulose in the EPS matrix. This combination strengthens the biofilm's physical and chemical barrier, making it more robust against external challenges. In contrast, biofilm morphotypes containing only cellulose or curli fimbriae do not achieve the same resistance level [7].

The genes, *dam* (deoxy adenine methylase) and *seqA* (sequestration A) play a role in the regulation of many bacterial properties, such as pathogenicity and virulence, and especially the replication time in bacteria [8]. Regulatory proteins produced from the genes in question generally perform these functions by binding sequentially to the 5'GATC3' target series [9, 10]. The SeqA protein and Dam methylase enzyme have been demonstrated to regulate the transcription of specific genes through the action of GATC methylation or by acting as co-activators. The results of mutation studies conducted on these genes indicated a notable reduction in the adhesion and invasion of *Salmonella* into host cells [11–15]. Studies conducted by our research group have determined that the genes in question significantly affect the biofilms formed by *Salmonella* in the solid-air and liquid-air intermediate phases. In these studies, in addition to mutant strains, the accuracy of the results was checked by using complementary constructs made with mutant genes using expression plasmids [16–18]. However, EPS analyses based on dye reactions do not allow the precise identification of quantitative changes in the EPS structure of the biofilm.

FT-IR and Raman spectroscopy are complementary techniques typically called vibrational spectroscopy. Both methods are simple, fast, non-destructive, and specific, providing fingerprint spectra and real-time analytical methods for analyzing molecules in different states [19]. FT-IR and Raman Scattering Spectroscopy methods are powerful and allow the identification of differences in microbial cells, primarily based on outer membrane cell components. These methods enable qualitative and quantitative identification of surface proteins, nucleic acids, carbohydrates, lipids, and humic structures [20]. In both methods, evaluation is made based on the infrared absorption and emission spectra of microbial cells [21]. Although Raman and FT-IR generally provide complementary information for each other in microbial cells, Raman and FT-IR bands are mutually exclusive when the target molecules have a translation center. FT-IR is especially recommended for functional groups with strong dipole shifts, and Raman spectra are recommended for functional groups with weak dipole shifts and strong symmetry [22].

As stated before, morphotyping *Salmonella* biofilms is challenging in scientific and practical terms. For this reason, methods with stronger qualitative and quantitative diagnostic capacity than dye reactions have been used. This study aims to characterize the molecular basis of the differences in biofilm production between the *dam* and *seqA* mutants and the wild strain with Raman and FT-IR spectroscopy and to determine the basic molecular targets in *S.* Typhimurium biofilms.

## Materials and methods

### Bacteria and culture conditions

*S.* Typhimurium DMC4 wild-type strain was used in the study. Planktonic forms of the *dam* and *seqA* gene mutants (Δ*dam and* Δ*seqA*) of this strain were produced at 200 RPM at 37 °C in Luria-Bertani (LB) broth for 18 h [16]. For biofilm structures, 48 h of incubation were applied at 20 °C [23, 24] at static conditions in salt-free LB ($LB^{-NaCl}$). 100 µg/ml of ampicillin was added to the Δ*dam* LB medium, and 25 µg/mL of chloramphenicol was added to the LB medium

for Δ*seqA*. Stock cultures were preserved at -80 °C in LB, with 60% glycerol.

## Biofilm assays

Biofilm assays in wild-type and mutant strains were grown in LB broth media without NaCl ($LB^{-NaCl}$). and in 96-well microtiter plates at 20 °C and static conditions. 30 µL of active culture was transferred to wells containing 100 µL $LB^{-NaCl}$ medium. Plates were incubated under static conditions for 24, 48, and 72 h. The wells were aspirated and then washed three times with 1X PBS. Subsequently, 130 µL of 95% methanol was added to each well to fix the biofilm forms adhering to the polystyrene surfaces. Following a 30-minute incubation period at room temperature, the wells were aspirated. Later, the plates were dried at room temperature, and 130 µL of 1% crystal violet was added to the wells and incubated at room temperature for 30 min. After, these plates were washed three times with sterile distilled water, and 130 µL of glacial acetic acid (33% v/v) was added to each well, and measurements were taken at $OD_{595}$. The result for each strain was calculated by subtracting the mean $OD_{595}$ of the biological replica of the control (LB broth only) from the mean $OD_{595}$ of the three biological replicates of the sample [25].

## Biofilm morphotype

Biofilm morphotypes were determined based on whether curli fimbriae and cellulose were present in the biofilm matrix. Congo Red and Calcofluor were used as indicator dyes to identify curli fimbria and cellulose, respectively. The optical density of *S.* Typhimurium active cultures was set at $OD_{600} = 3.0$, and 5 µl of bacterial suspension was dropped onto $LB^{-NaCl}$ agar containing 40 µg/mL of Congo Red (Sigma-Aldrich, USA). To determine the presence of cellulose, active cultures were transferred onto $LB^{-NaCl}$ agar containing 20 µg/mL of Calcofluor (Sigma-Aldrich, USA). To evaluate the pellicle-forming properties of the strains, 500 µL of the active culture was added to 4.5 mL of $LB^{-NaCl}$ medium. Ring formation of the strains in the liquid-air interphase was observed daily. The results were evaluated after 8 days of incubation at 20 °C, and biofilm morphotypes were observed under a stereomicroscope (Leica, Germany) [26].

## Swimming and swarming motility

To assess the 'swimming' motility, *S.* Typhimurium strains were initially cultured overnight at 37°C in LB agar. After incubation, one colony was selected from the agar and transferred to a 0.3% LB agar surface. The sample was then incubated for 9 hours at 20°C, 28°C, and 37°C. To assess the 'Swarming' motility, the strains were incubated overnight on LB agar at 37 °C. Following incubation, a single isolated colony was selected from the agar surface and introduced into 0.5% LB agar supplemented with 0.5% glucose. The agar plates were assessed by incubating at 20 °C, 28 °C, and 37 °C for 9 h. The distance between the inoculation zone on the agar plates and the outer boundary of the 'swimming' and 'swarming' zone was assessed using measurement [27].

## FT-IR Spectroscopy

In trials, the biofilm structures created on polystyrene surfaces were subjected to a lyophilization process and made ready for FT-IR analyses by applying optimum biofilm formation temperature and duration (72 h at 20 °C) in $LB^{-NaCl}$ media. The FT-IR spectra of these structures were recorded in the middle IR (4500–850 $cm^{-1}$) region using the universal tensor 27 FT-IR (4500–850 $cm^{-1}$) by using the ATR cell (Pike Technologies, Wisconsin, USA), which contains the mercury cadmium telluride detector and the ZNSE crystal. Three measurements were performed for each technical sample, and arithmetic averages were used in advanced analysis. OPUS 5.5 (Bruker) software was used for spectra analysis. Statistical significance is determined by ANOVA analysis [28].

## Raman spectroscopy

Biofilm forms of *S.* Typhimurium DMC4 strain and its *dam* and *seqA* gene mutants were obtained after 72 h of incubation of cultures inoculated at 20 °C to $LB^{-NaCl}$ broth media. The biofilm structure in this media was washed with sterile distilled water three times after being carefully collected through sterile forceps. Biofilm preparations were dried at room temperature at the last stage, and argon laser power settings were performed in the Raman spectrophotometer (1.5 mV of 514 nm). After the samples were placed on a Raman spectrophotometer, measurements were performed in the range of 2000–200 $cm^{-1}$ [29].

## Statistical analysis

Statistical analysis was performed using GraphPad Prism 8. A one-way ANOVA test was used to determine whether the differences between groups were statistically significant ($p < 0.05$). Tukey's exact test was used to assess group differences.

## Results and discussion

### Biofilm assays

The *S.* Typhimurium wild-type strain and mutants reached the maximum biofilm production rate at the end of 72 h. At all incubation times, biofilm production levels in *dam* and *seqA* mutants were lower than in the wild-type strain. The *seqA* mutant showed the lowest level of biofilm formation (Fig. 1).

These results indicate that both *dam* and *seqA* genes are effective in the biofilm formation ability in the *S.* Typhimurium DMC4 strain. In the studies conducted to date, it has been determined that *dam* and *seqA* genes participate in the regulation of biofilm structures as well as pathogenicity, virulence, regulation of DNA replication time, and similar properties in *Salmonella* serovars [16].

'rdar' biofilm morphotype was determined for wild-type strain and *dam* and *seqA* mutants at 20 °C on LB agar containing Congo Red after 8 days. The degree of red color observed in morphotypes is dependent on the quantity of curli fimbriae production [30]. The observed color difference in the Δ*seqA* strain explains this situation. Pellicles are defined as biofilm structures formed at the liquid-air interface. All strains used in the study demonstrated the capacity to form pellicles. The structure is rigid in the wild-type strain, but it is quite fragile in the Δ*seqA* strain.

In the assay conducted with calcofluor, the highest fluorescence in both solid and liquid media was observed in the wild-type strain and the lowest in the Δ*seqA* strain. Differences were observed in the swimming and swarming movements depending on the incubation temperatures. Bacteria inoculated on nutrient media containing agar move towards nutrient-rich areas in parallel with the depletion of nutrients in the first inoculated area. Optimum swimming and swarming movements were observed in all strains after a 10-hour incubation period at 37 °C. Movement was significantly reduced at lower temperatures (28 and 20 °C). When the DMC4 wild-type strain and its *dam* and *seqA* gene mutant strains were compared, it was observed that swimming and swarming movements, respectively, decreased at all incubation temperatures (Fig. 2).

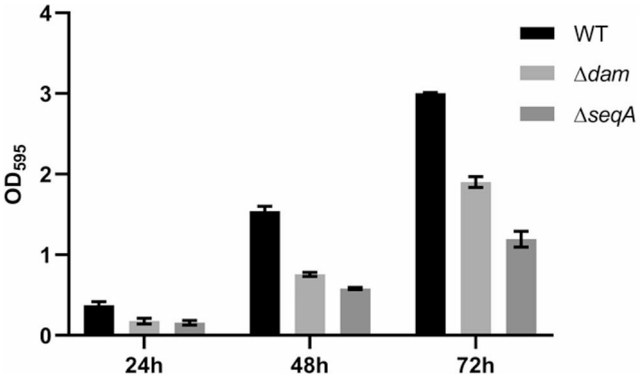


**Fig. 1** Changes of biofilm production in *S.* Typhimurium DMC4 wild-type strain and its *dam* and *seqA* mutants according to the incubation period

### FT-IR Spectra analysis

Differences in lipid, protein, and carbohydrate densities were analyzed in the FT-IR spectrum (Fig. 3). Symmetric and asymmetric C-H groups between 3000–2800 $cm^{-1}$ regions show the lipid density in bacterial cell walls and membranes [31]. The lipid densities and diversity of the mature biofilm structures of the wild-type strain decreased significantly ($p < 0.05$) in the *dam* and *seqA* mutants. The lowest lipid density was found in the *seqA* mutant (Fig. 3). When evaluated in terms of protein contents, the amide I (1700–1600 $cm^{-1}$) densities of the mutant strains decreased in comparison to the wild-type strain, while the amide II (1600–1500 $cm^{-1}$) [32, 33] densities increased. This shows that the protein contents of the biofilm structures of *dam* and *seqA* mutants changed in quality and quantity when compared to the wild-type strain ($p < 0.05$) (Fig. 3). The data indicated that curli fimbriae went through structural deformation and function loss in the *dam* and *seqA* mutants. It is known that amide I bonds are concentrated in the alpha helix structures, which are the structural indicators of amyloid proteins, including the curli fimbriae. Additionally, amide II bands are concentrated in the beta sheets, where these proteins are disrupted [34]. On the other hand, it was determined that the glucose (1046–999 $cm^{-1}$) contents in the biofilm structures of all strains used in the study differed, and that glucose concentrations in the *dam* and *seqA* mutants decreased significantly compared to the wild-type strain (Fig. 3). The same situation was detected in (1→3)-α-D-glucans (929 $cm^{-1}$). All FT-IR data, when interpreted together with the data obtained from phenotypic tests, show that the biofilm structures formed by the mutant strains have undergone severe changes in terms of proteins, lipids, and carbohydrates compared to the wild-type strain, and these changes significantly change the biofilm structure and function.

### Raman Spectra analysis

The samples were subjected to Raman spectra analyses to test the compatibility of FT-IR data and elements that could not be identified in detail in FT-IR spectra analyses. As a result of these examinations, significant changes were observed in the peak points of the Raman spectrum, such as lipid, amide bonds, phosphodiester bonds, glycosidic bonds, and glucans in the biofilm structures formed by

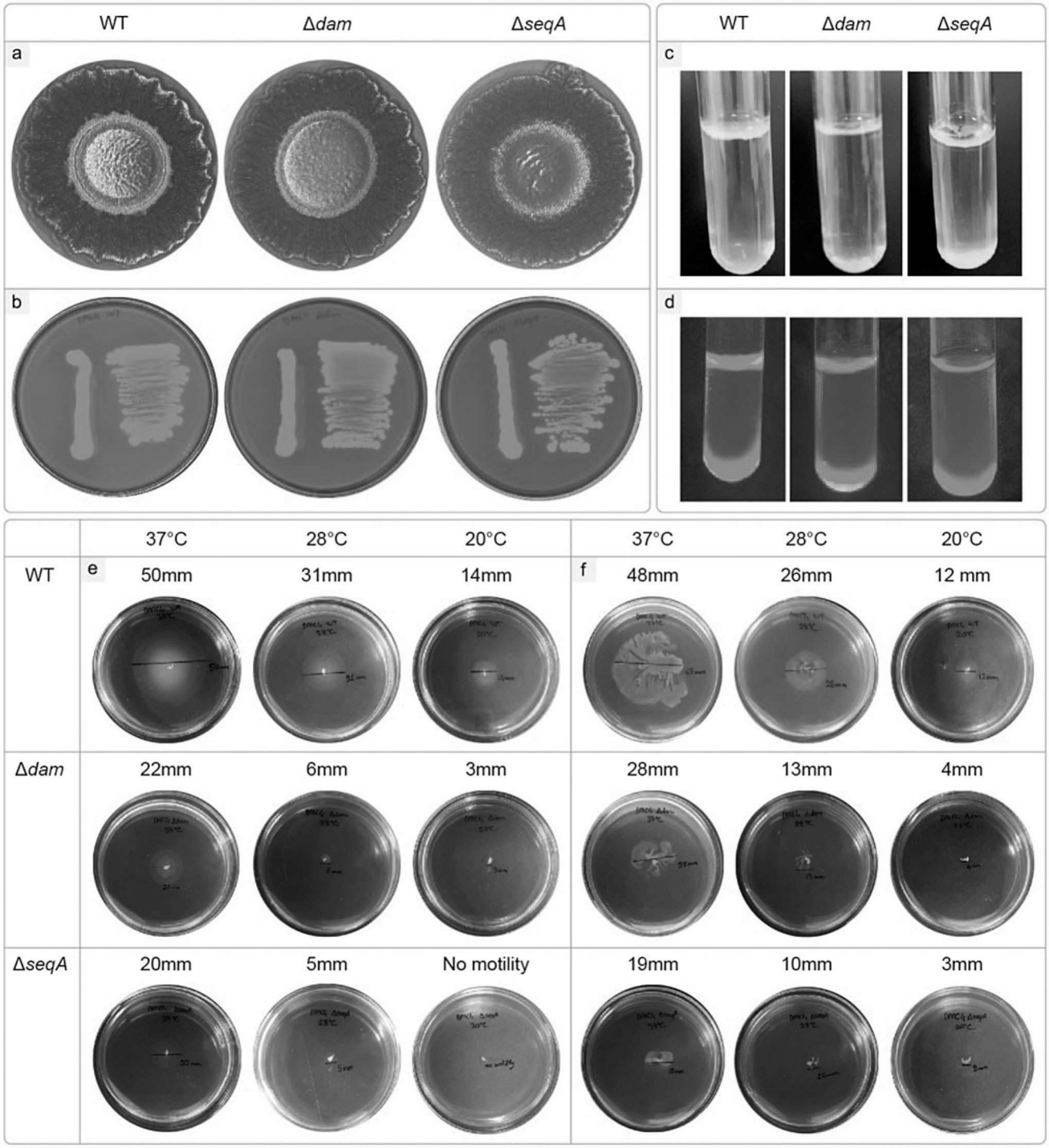


**Fig. 2** Biofilm phenotypes of DMC4 wild-type, Δ*dam*, and Δ*seqA* mutants. **a**) Stereo-microscope images of biofilm morphotypes. **b**) Calcofluor binding of *Salmonella* strains. **c**) Pellicle-forming properties on glass tubes. **d**) Staining of pellicle structure with Calcofluor in liquid. **e**) Swimming motility. **f**) Swarming motility

the *S.* Typhimurium DMC4 wild-type strain and its Δ*dam* and Δ*seqA* strains. Table 1 presents the main characteristics observed in the Raman spectra of bacterial biofilm, as shown in Fig. 4.

It has been determined that bacterial surface components and extracellular structures (especially flagella, lipopolysaccharides, and exopolysaccharides) are crucial for autoaggregation and biofilm production in many bacterial species [35, 36]. In the generally accepted model of biofilm formation,

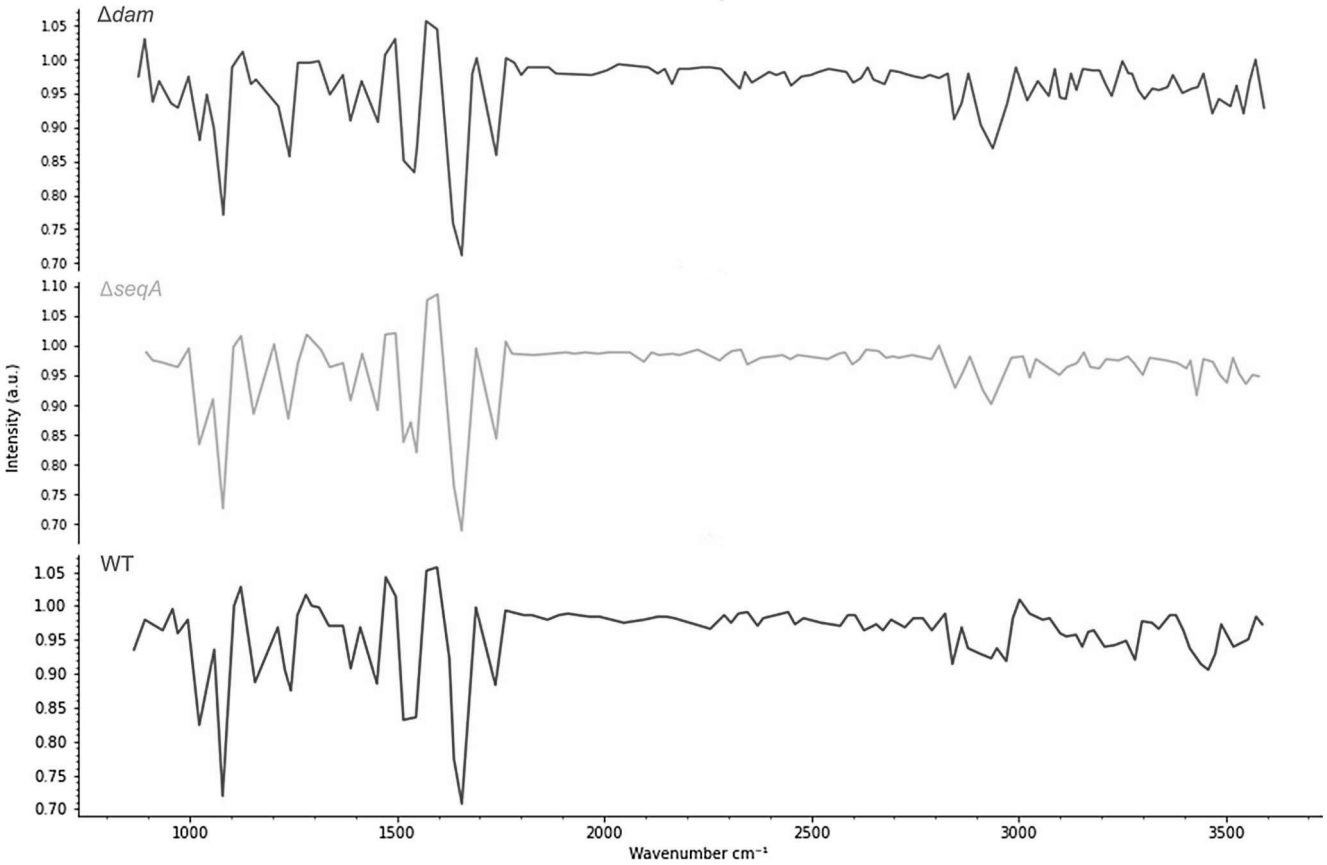


**Fig. 3** FT-IR spectra of DMC4, Δ*dam*, and Δ*seqA* mutant bacterial biofilms are compared regarding representative relative intensity

**Table 1** Assignments of principal infrared vibrational bands of the 3000–900 $cm^{-1}$ region of the FT-IR spectrum [33]

| FT-IR Wavenumber ($cm^{-1}$) | Description* |
|---|---|
| 2950–2960 | $\nu_{as}$ ($CH_3$), lipids |
| 2920–2940 | $\nu_{as}$ ($CH_2$), lipids |
| 2850–2860 | $\nu_s$ ($CH_2$), lipids |
| 1700 – 1600 | 80% ν (C = O), 20% (C-N), τ (HOH), Amide I, water |
| 1600 – 1500 | 60% τ (N–H), 30% (C–N), 10% ν (C–C), Amide II |
| 1400 – 1350 | $\delta_s$ ($CH_3$), $\delta_s$ ($CH_2$), $\nu_s$ (C = O), proteins, lipids |
| 1046 – 999 | Skeletal vibration connected to the anomeric structure of D-glucose |
| 929 | (1⟶3)-α-D-glucan |

*ν: stretching, δ: deformational, τ: bending, as asymmetrical, s: symmetrical

environmental signals trigger the process and are critical for the flagellar biofilm community to achieve surface-approaching movement. The initial stages of adhesion to the surface are mediated by outer membrane proteins (e.g., calcium-binding proteins), pili, or LPS (lipopolysaccharides) [37]. On the other hand, the main components of the EPS, which is the fundamental structural and functional element of biofilm structures, include exopolysaccharides, extracellular DNA (eDNA) and RNA (eRNA) [38], proteins, lipids, and water [39]. EPS stabilizes the architectural form and three-dimensional structure of biofilms [37]. The ability of cells in the biofilm to change the membrane lipid composition is a critical adaptation to environmental stress factors for biofilm development [40].

Raman spectra attributed to the presence of the hydrocarbon chain in three spectroscopic regions (1500–1400 $cm^{-1}$, 1300–1250 $cm^{-1}$, and 1200–1050 $cm^{-1}$) [33, 41] (Table 2). The highest intensity of the 1445–1461 $cm^{-1}$ bands indicates saturated lipids [42]. Density differences in these bands refer to changes in lipid amounts and saturation of fatty acids during the maturation phase and biofilm composition [33]. Raman data obtained in our study clearly shows that the amount of lipids and, therefore, the lipid composition in the biofilm structure of the wild-type strain decreases dramatically in the *dam* and *seqA* mutants (Fig. 4). This finding, which phenotypic tests cannot identify, is of critical importance in the disruption of biofilm structure and function in these mutants.

In Raman spectra, ~783 $cm^{-1}$ represents phosphodiester bonds in DNA, and 1340–1330 $cm^{-1}$ represents

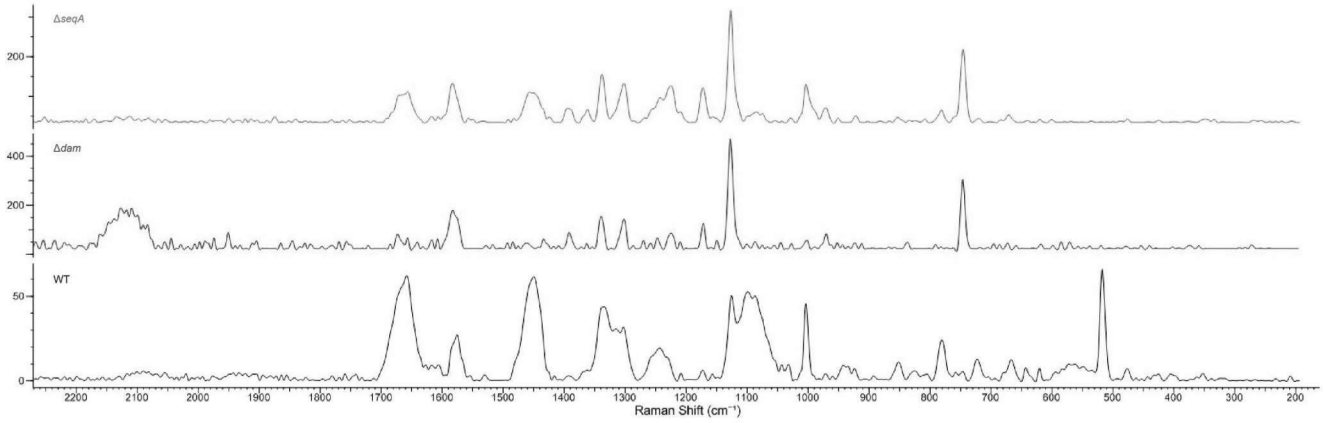


**Fig. 4** Raman spectra of DMC4, Δ*dam*, and Δ*seqA* mutant bacterial biofilms are compared in terms of representative relative intensity

**Table 2** Significant bands and vibration types associated with specific components appear in the Raman spectra of the biofilm samples [33]

| Raman Shift ($cm^{-1}$) | Description* |
|---|---|
| 1700 – 1600 | ν (C = O), Amide I |
| 1600 – 1500 | ν (C-N), δ (N–H), Amide II |
| 1500 – 1400 | in-plane τ and out-of-plane τ ($CH_2$), lipids |
| 1445–1461 | $\nu_s$ ($CH_2$), saturated lipids |
| 1340 – 1330 | polynucleotide chains, DNA purine bases |
| 1300 – 1250 | in-plane τ and out-of-plane τ ($CH_3$), lipids |
| 1200 – 1050 | ν (C-C), lipids |
| ~1094 | $\nu_{as}$ (COC), (1→4)-β-linked glycosidic bonds |
| ~1000 | phenylalanine ring breathing |
| 800 – 640 | out-of-plane τ (N-H), Amide V |
| ~783 | ring breathing of cytosine, thymine, uracil; $\nu_s$ (O-P-O), phosphodiester bonds in DNA |
| 770 – 625 | τ (O = C-N), Amide IV |
| ~520 | Glucans |

*$\nu$: stretching, $\delta$: deformational, $\tau$: bending, as asymmetrical, s: symmetrical

polynucleotide chains and DNA purine bases [33]. The decreases in the Raman intensities of *seqA* and *dam* mutants in these regions compared to the wild-type strain *S.* Typhimurium DMC4, respectively (Fig. 4), are a sign of the reduced amount of eDNA in the biofilm matrix of these mutants. These findings provide indirect evidence for the role of eDNA in biofilm structures, which is still controversial, but has been described to hold the main elements together in mature biofilm structures [43, 44].

As protein structures mature, protein-related peaks emerge. Previous studies have suggested that the phenylalanine band observed at 1000 $cm^{-1}$ may be an essential indicator for detecting biofilms with protein structure [45]. This band, which was at high intensity in the wild-type strain, was observed to be at decreasing intensity in the *seqA* and *dam* mutants, respectively. Amide I (1700–1600 $cm^{-1}$) and Amide II (1600–1500 $cm^{-1}$) bands are sensitive to changes in the secondary structures of proteins. These bands are associated with proteins formed by the combination of CO=(νr = O) stretching and N-H (δN-H) cracking of amides [46–48]. Amide peaks can be associated with alpha helix and disordered helical structures of cellular proteins, revealing the presence of beta sheets [49]. This shows that biofilms consist of alpha helices and beta sheets secondary structures. It was determined that the 800–640 $cm^{-1}$ peaks (amide V) were at higher intensity in the wild-type strain compared to the mutant strains. 770–625 $cm^{-1}$ peaks (amide IV) were detected at higher intensity in mutant strains than in the wild-type strain (Fig. 4). The Raman spectra obtained prove that the protein ratios and compositions in the biofilm structures of the wild-type strain and the mutant vary. The most critical components in *Salmonella* biofilms are the curli fimbria proteins and cellulose, which determine the main functions of the EPS matrix [50]. When all the data above are interpreted together with FT-IR results, it shows that curli fimbriae structurally changed and reduced at a critical level along with other protein structures in the biofilm structures of mutant strains.

UDP- produces glucan chains by glycosylating glucose [51]. Bacterial glucan refers to a class of EPS that includes a group of polysaccharides naturally occurring in the cell walls of various bacteria, with different physicochemical properties depending on the source and structure [52]. In addition to creating protective and highly acidic microenvironments, glucans help promote bacterial adhesion and cohesion, interactions between species, and biofilm accumulation [39, 53, 54]. While the Raman intensity of glucan at approximately 520 $cm^{-1}$ was relatively high in the wild-type strain, the intensity was found to be quite low in *the dam* and *seqA* mutants. Polysaccharides, especially (1→3), (1→6)-α-D-glucans, have structural and functional roles in the biofilm matrix [55]. Cellulose is a polymer consisting of glucose units connected by (1→4)-β glycosidic

bonds [56]. The band corresponding to the stretching of the glycosidic bond in the backbone of the cellulose structure ((1→4)-β-linked glycosidic bonds) is approximately 1094. In this region, the highest Raman density was determined in the wild-type strain, which is a strong biofilm producer. In this sense, the highest decrease was detected in the *seqA* mutant. These data (Fig. 4) show that cellulose production is significantly reduced in the biofilm structures of mutant strains, which corroborated to the calcofluor experiments performed.

Finally, the generalizations that fimbrial and flagellar structures are the main factors of the swimming movement in planktonic bacterial forms, and that the cellulose in EPS plays an active role in the swarming movement are also valid in *Salmonella* due to the significant decreases in protein and cellulose ratios in the mutants used in the study.

## Conclusions

In conclusion, *dam* and *seqA S.* Typhimurium DMC4 mutants had a markedly reduced ability for biofilm formation, associated with a reduction of the content of macromolecules, especially β-glucans and amides. These changes were successfully demonstrated by FT-IR and Raman spectral analyses, which show how analytical techniques allow the identification of key molecular changes in the structural components of the biofilm matrix. Together, these findings may contribute to a potential targeted intervention against the challenge posed by *S.* Typhimurium biofilms.

**Authors contribution** All authors contributed to the study's conception and design. Material preparation, data collection, and analysis were performed by Caner ÖZDEMİR, İbrahim ERDOĞAN, Kağan ÖZDEMİR, Nefise AKÇELİK and Mustafa AKÇELİK. The first draft of the manuscript was written by Mustafa AKÇELİK, and all authors commented on previous versions of the manuscript. All authors read and approved the final manuscript.

### Declarations

**Ethical approval** Not applicable.

**Financial interest** No funding was received for conducting this study.

**Competing interests** Authors declare no conflict of interest.

## References

1. Kim SH, Wei CI (2009) Molecular characterization of biofilm formation and attachment of *Salmonella enterica* Serovar Typhimurium DT104 on food contact surfaces. JPF 72(9):1841–1847. https://doi.org/10.4315/0362-028X-72.9.1841
2. Speranza B, Corbo MR, Sinigaglia M (2011) Effects of nutritional and environmental conditions on *Salmonella* sp. biofilm formation. J Food Sci 76(1):M12–M16. https://doi.org/10.1111/j.1750-3841.2010.01936.x
3. Donlan RM (2002) Biofilms: microbial life on surfaces. Emerg Infect Dis 8(9):881–890. https://doi.org/10.3201/eid0809.020063
4. Flemming HC, Wingender J (2010) The biofilm matrix. Nat Rev Microbiol 8:623–633. https://doi.org/10.1038/nrmicro2415
5. Steenackers H, Hermans K, Vanderleyden J et al (2012) *Salmonella* biofilms: an overview on occurrence, structure, regulation and eradication. Food Res Int 45:502–531. https://doi.org/10.1016/j.foodres.2011.01.038
6. Hall CW, Mah T (2017) Molecular mechanisms of biofilm-based antibiotic resistance and tolerance in pathogenic bacteria. FEMS Microbiol Rev 41(3):276–301. https://doi.org/10.1093/femsre/fux010
7. Hobley L, Harkins C, MacPhee CE, Stanley-Wall NR (2015) Giving structure to the biofilm matrix: an overview of individual strategies and emerging common themes. FEMS Microbiol Rev 39(5):649–669. https://doi.org/10.1093/femsre/fuv015
8. Lobner-Olesen A, Marinus MG, Hansen FG (2003) Role of SeqA and dam in *Escherichia coli* gene expression: a global/microarray analysis. Proc Natl Acad Sci USA 100(8):4672–4677. https://doi.org/10.1073/pnas.0538053100
9. Aloui A, Mihoub M, Sethom MM, Chatti A, Feki M, Kaabachi N, Landoulsi A (2010) Effects of the *dam* and/or *seqA* mutations on the fatty acid and phospholipid membrane composition of *Salmonella enterica* Serovar Typhimurium. Foodborne Pathog Dis 7:573–583. https://doi.org/10.1089/fpd.2009.0385
10. Chatti A, Messaoudi N, Mihoub M, Landoulsi A (2012) Effects of hydrogen peroxide on the motility, catalase and superoxide dismutase of *dam* and/or *seqA* mutant of *Salmonella* Typhimurium. World J Microbiol Biotechnol 28:129–133. https://doi.org/10.1007/s11274-011-0801-8
11. García-del-Portillo F, Pucciarelli MG, Casadesús J (1999) DNA adenine methylase mutants of *Salmonella* Typhimurium are deficient in protein secretion, cell invasion and M cell cytotoxicity. PNAS 96:11584–11588. https://doi.org/10.1073/pnas.96.20.11578
12. Heithoff DM, Sinsheimer RL, Low DA, Mahan MJ (1999) An essential role for DNA adenine methylation in bacterial virulence. Science 284:967–970. https://doi.org/10.1126/science.284.5416.967
13. Chatti A, Daghfous D, Landoulsi A (2007) Effect of *seqA* mutation on *Salmonella* Typhimurium virulence. J Infect 54:241–245. https://doi.org/10.1016/j.jinf.2007.01.002
14. Jakomin M, Chessa D, Baumler AJ, Casadesus J (2008) Regulation of the *Salmonella enterica Std* fimbrial operon by DNA adenine methylation, SeqA, and HdfR. J Bacteriol 190:7406–7413. https://doi.org/10.1128/JB.01136-08
15. Chatti A, Aloui M, Tagourti J, Mihoub M, Landoulsi A (2014) Novobiocin sensitivity of *Salmonella* Typhimurium *dam* and/or *seqA* mutants. Pol J Microbiol 63:51–56
16. Uğur S, Akçelik N, Yüksel FN, Taşkale Karatuğ N, Akçelik M (2018) Effects of *dam* and *seqA* genes on biofilm and pellicle formation in *Salmonella*. Pathog Glob Health 112(7):368–377. https://doi.org/10.1080/20477724.2018.1539803
17. Has EG, Akçelik N, Akçelik M (2023) Comparative global gene expression analysis of biofilm forms of *Salmonella* Typhimurium ATCC 14028 and its *seqA* mutant. Gene 853:147094. https://doi.org/10.1016/j.gene.2022.147094
18. Oğuz SK, Has EG, Akçelik N, Akçelik M (2023) Phenotypic impacts and genetic regulation characteristics of the DNA adenine methylase gene (*dam*) in *Salmonella* Typhimurium biofilm forms. Res Microbiol 174(1–2):103991. https://doi.org/10.1016/j.resmic.2022.103991
19. Rohman A, Windarsih A, Lukitaningsih E, Rafi M, Betania K, Fadzillah NA (2019) The use of FTIR and Raman spectroscopy in

combination with chemometrics for analysis of biomolecules in biomedical fluids: a review. Biomed Spectrosc Ima 8(3–4):55–71. https://doi.org/10.3233/BSI-200189
20. Harz M, Rösch P, Popp J (2009) Vibrational spectroscopy—A powerful tool for the rapid identification of microbial cells at the single-cell level. Cytometry A 75A(2):104–113. https://doi.org/10.1002/cyto.a.20682
21. Kassem A, Abbas L, Coutinho O, Opara S, Najaf H, Kasperek D, Pokhrel K, Li X (2023) Applications of Fourier Transform-Infrared spectroscopy in microbial cell biology and environmental microbiology: advances, challenges, and future perspectives. Front Microbiol 14:1304081. https://doi.org/10.3389/fmicb.2023.1304081
22. Gao F, Ben-Amotz D, Yang Z, Han L, Liu X (2021) Complementarity of FT-IR and Raman spectroscopies for the species discrimination of meat and bone meals related to lipid molecular profiles. Food Chem 345:128754. https://doi.org/10.1016/j.foodchem.2020.128754
23. Lamas A, Fernandez-No IC, Miranda JM, Vázquez B, Cepeda A, Franco CM (2016) Biofilm formation and morphotypes of *Salmonella enterica* subsp. Arizonae differs from those of other *Salmonella enterica* subspecies in isolates from poultry houses. J Food Prot 79(7):1127–1134. https://doi.org/10.4315/0362-028X.JFP-15-568
24. Roy PK, Ha AJW, Mizan MFR et al (2021) Effects of environmental conditions (temperature, pH, and glucose) on biofilm formation of *Salmonella enterica* serotype Kentucky and virulence gene expression. Poult Sci 100(7):101209. https://doi.org/10.1016/j.psj.2021.101209
25. Vestby LK, Moretro T, Langsrud S, Heir E, Nesse LL (2009) Biofilm forming abilities of *Salmonella* are correlated with persistence in fish meal and feed factories. BMC Vet Res 5(20):1–6. https://doi.org/10.1186/1746-6148-5-20
26. Wang F, Deng L, Huang F, Wang Z, Lu Q, Xu C (2020) Flagellar motility is critical for *Salmonella enterica* serovar typhimurium biofilm development. Front Microbiol 11:1695. https://doi.org/10.3389/fmicb.2020.01695
27. Ahmad I, Rouf SF, Sun L, Cimdins A, Shafeeq S, Guyon SL, Schottkowski M, Rhen M, Römling U (2016) BcsZ inhibits biofilm phenotypes and promotes virulence by blocking cellulose production in *Salmonella enterica* Serovar Typhimurium. Microb Cell Fact 15:177. https://doi.org/10.1186/s12934-016-0576-6
28. Ariafar MN, Iğci N, Akçelik M, Akçelik N (2019) Investigation of the effect of different environmental conditions on biofilm structure of *Salmonella enterica* serotype Virchow via FTIR spectroscopy. Arch Microbiol 91233–1248. https://doi.org/10.1007/s00203-019-01681-5
29. Hlaing MM, Dunn M, Stoddart PR, McArthur SL (2016) Raman spectroscopic identification of single bacterial cells at different stages of their lifecycle. Vib Spectrosc 86:81–89. https://doi.org/10.1016/j.vibspec.2016.06.008
30. Wen Y, Ouyang Z, Devreese B, He W, Shao Y, Lu W, Zheng F (2017) Crystal structure of master biofilm regulator CsgD regulatory domain reveals an atypical receiver domain. Protein Sci 26(10):2073–2082. https://doi.org/10.1002/pro.3245
31. Derenne A, Vandersleyen O, Goormaghtigh E (2014) Lipid quantification method using FTIR spectroscopy applied on cancer cell extracts. Biochim Biophys Acta 1841(8):1200–1209. https://doi.org/10.1016/j.bbalip.2013.10.010
32. Sabbatini S, Conti C, Orilisi G, Giorgini E (2017) Infrared spectroscopy as a new tool for studying single living cells: is there a niche? Biomed Spectrosc Imaging 6:85–99. https://doi.org/10.3233/BSI-170171
33. Gieroba B, Krysa M, Wojtowicz K, Wiater A et al (2020) The FT-IR and Raman spectroscopies as tools for biofilm characterization created by cariogenic streptococci. Int J Mol Sci 21(11):3811. https://doi.org/10.3390/ijms21113811
34. Hauptmann A, Hoelzl G, Mueller M, Bechtold-Peters K, Loerting T (2022) Raman marker bands for secondary structure changes of frozen therapeutic monoclonal antibody formulations during thawing. J Pharm Sci 112(1):51–60. https://doi.org/10.1016/j.xphs.2022.10.015
35. Costerton JW, Lewandowski Z, Caldwell DE, Korber DR, Lappin-Scott HM (1995) Microbial biofilms. Annu Rev Microbiol 49(1):711–745. https://doi.org/10.1146/annurev.mi.49.100195.003431
36. Schembri MA, Christiansen G, Klemm P (2001) FimH-mediated autoaggregation of *Escherichia coli*. Mol Microbiol 41(6):1419–1430. https://doi.org/10.1046/j.1365-2958.2001.02613.x
37. Bogino PC, Oliva MM, Sorroche FG, Giordano W (2013) The role of bacterial biofilms and surface components in plant-bacterial associations. Int J Mol Sci 14(8):15838–15859. https://doi.org/10.3390/ijms140815838
38. Flemming HC, Wingender J, Szewzyk U, Steinberg P, Rice SA, Kjelleberg S (2016) Biofilms: an emergent form of bacterial life. Nat Rev Microbiol 14(9):563–575. https://doi.org/10.1038/nrmicro.2016.94
39. Karygianni L, Ren Z, Koo H, Thurnheer T (2020) Biofilm matrixome: extracellular components in structured microbial communities. Trends Microbiol 28(8):668–681. https://doi.org/10.1016/j.tim.2020.03.016
40. Alim D, Sircaik S, Panwar SL (2018) The significance of lipids to biofilm formation in *Candida albicans*: an emerging perspective. J Fungi 4(4):140. https://doi.org/10.3390/jof4040140
41. Czamara K, Majzner K, Pacia MZ, Kochan K, Kaczor A, Baranska M (2015) Raman spectroscopy of lipids: a review. J Raman Spectrosc 46(1):4–20. https://doi.org/10.1002/jrs.4607
42. Verma SP, Wallach DF (1977) Raman Spectra of some saturated, unsaturated, and deuterated $C_{18}$ fatty acids in the HCH-deformation and CH-stretching regions. Biochim Biophys Acta (BBA)-Lipids Lipid Metabolism 486(2):217–227. https://doi.org/10.1016/0005-2760(77)90018-2
43. Whitchurch CB, Tolker-Nielsen T, Ragas PC, Mattick JS (2002) Extracellular DNA required for bacterial biofilm formation. Science 295(5559):1487. https://doi.org/10.1126/science.295.5559
44. Seviour T, Winnerdy FR, Wong LL et al (2021) The biofilm matrix scaffold of *Pseudomonas aeruginosa* contains G-quadruplex extracellular DNA structures. Npj Biofilms Microbiomes 7(1):27. https://doi.org/10.1038/s41522-021-00197-5
45. Keleştemur S, Avci E, Çulha M (2018) Raman and surface-enhanced Raman scattering for biofilm characterization. Chemosensors 6(1):5. https://doi.org/10.3390/chemosensors6010005
46. Jiao Y, Cody GD, Harding AK, Wilmes P, Schrenk M, Wheeler KE, Banfield JF, Thelen MP (2010) Characterization of extracellular polymeric substances from acidophilic microbial biofilms. Appl Environ Microbiol 76(9):2916–2922. https://doi.org/10.1128/AEM.02289-09
47. Ojeda JJ, Dittrich M (2012) Fourier transform infrared spectroscopy for molecular analysis of microbial cells. Methods Mol Biol 881:187–211. https://doi.org/10.1007/978-1-61779-827-6_8
48. Baker MJ, Trevisan J, Bassan P, Bhargava R et al (2014) Using Fourier transform IR spectroscopy to analyze biological materials. Nat Protoc 9(8):1771–1791. https://doi.org/10.1038/nprot.2014.110
49. Barth A (2017) Infrared spectroscopy of proteins. Biochim Biophys Acta 1767(9):1073–1101. https://doi.org/10.1016/j.bbabio.2007.06.004
50. Römling U, Rohde M, Olsén A, Normark S, Reinköster J (2000) AgfD, the checkpoint of multicellular and aggregative behaviour in *Salmonella* Typhimurium regulates at least two independent

pathways. Mol Microbiol 36(1):10–23. https://doi.org/10.1046/j.1365-2958.2000.01822.x
51. Solano C, García B, Valle J, Berasain C, Ghigo J, Gamazo C, Lasa I (2002) Genetic analysis of *Salmonella enteritidis* biofilm formation: critical role of cellulose. Mol Microbiol 43:793–808. https://doi.org/10.1046/j.1365-2958.2002.02802.x
52. Xu L, Zhang J (2016) Bacterial glucans: production, properties, and applications. App Microbiol Biotechnol 100(21):9023–9036. https://doi.org/10.1007/s00253-016-7836-6
53. Zhu F, Zhang H, Wu H (2015) Glycosyltransferase-mediated sweet modification in oral streptococci. J Dent Res 94(5):659–665. https://doi.org/10.1177/0022034515574865
54. Bowen WH, Burne RA, Wu H, Koo H (2018) Oral biofilms: pathogens, matrix, and polymicrobial interactions in microenvironments. Trends Microbiol 26(3):229–242. https://doi.org/10.1016/j.tim.2017.09.008
55. Pleszczyńska M, Wiater A, Janczarek M, Szczodrak J (2015) (1→3)-α-D-Glucan hydrolases in dental biofilm prevention and control: a review. Int J Biol Macromol 79:761–778. https://doi.org/10.1016/j.ijbiomac.2015.05.052
56. O'Sullivan AC (1997) Cellulose: the structure slowly unravels. Cellulose 4:173–207. https://doi.org/10.1023/A:1018431705579

**Publisher's note** Springer Nature remains neutral with regard to jurisdictional claims in published maps and institutional affiliations.

Springer Nature or its licensor (e.g. a society or other partner) holds exclusive rights to this article under a publishing agreement with the author(s) or other rightsholder(s); author self-archiving of the accepted manuscript version of this article is solely governed by the terms of such publishing agreement and applicable law.